Available online at www.sciencedirect.com
SCIENCE DIRECT®
Journal of Solid State Chemistry 177 (2004) 800–805
JOURNAL OF SOLID STATE CHEMISTRY
http://elsevier.com/locate/jssc

Synthesis and crystal structure of two tin fluoride materials: $NaSnF_3$ (BING-12) and $Sn_3F_3PO_4$

Tolulope O. Salami, Peter Y. Zavalij, and Scott R.J. Oliver*

Department of Chemistry, State University of New York at Binghamton, Science II Building, Binghamton, NY 13902-6000, USA

Received 17 June 2003; received in revised form 29 August 2003; accepted 17 September 2003

Abstract

A new compound, sodium tin trifluoride ($NaSnF_3$, which we denote BING-12 for SUNY at Binghamton, Structure No. 12), was synthesized solvothermally from a pyridine–water solvent system. The new compound crystallized in the monoclinic space group $C2/c$ (No. 15), with $a = 11.7429(12)$ Å, $b = 17.0104(18)$ Å, $c = 6.8528(7)$ Å, $\beta = 100.6969(2)^\circ$, $V = 1345.1(2)$ Å^3 and $Z = 16$. The layered structure consists of outer pyramidal SnF_3 units, where the fluorides surround a central layer of six- and seven-coordinate sodium atoms. The layers are stabilized by charged Na^+ galleries that reside in the center of the layers. Tin trifluorophosphate ($Sn_3F_3PO_4$, Compound **2**) was isolated from a related synthetic system, and crystallized in the rhombohedral space group $R3$ (No. 146), with $a = 11.8647(11)$ Å, $c = 4.6291(6)$ Å, $V = 564.34(10)$ Å^3 and $Z = 3$. The framework is made up of helical –Sn–F– chains, which are connected by phosphate groups. The materials were characterized by powder X-ray diffraction (PXRD), variable temperature PXRD (VT-PXRD), thermogravimetric analysis (TGA) and scanning electron microscopy (SEM).

Keywords: Tin fluoride; Tin fluorophosphate; Sn-based layer; Solvothermal synthesis

1. Introduction

The synthesis of tin fluorides and phosphates has led to the development of materials with potential use in solar conversion, fuel cells, oxygen permeable membranes and solid electrolytes [1–3]. The typical synthetic techniques for Sn-based materials are solvothermal, high temperature and sol–gel. Solvothermal synthesis, which involves the use of a templating agent (e.g., large organic amines or surfactants), is a very attractive method and has led to the synthesis of numerous open materials, primarily anionic layers stabilized by positively charged ions [1–3].

Our group [4–9] as well as Cheetham and co-workers [10–20] have reported a wide array of open framework (3D), layered (2D) and chain (1D) Sn-based materials. The rich structural chemistry of Sn is attributed to its large range of possible coordination numbers (2–9), as well as geometry. This flexibility allows for the synthesis of new materials with interesting chemistry. We use traditional cationic templates, as well as non-traditional anionic templates in the form of inorganic or organic anions [4–9]. The latter are used to stabilize cationic inorganic materials [5].

Ternary tin sulfides with general formula $Sn_xS_yA_z$ (e.g. $Sn_2S_6P_2$; A represents any element other than tin or sulfur) show interesting geometry. This class of compounds contains tin–sulfur covalent bonds, with the Sn centers usually in the +4 oxidation state and half the metal sites often vacant. The Sn centers in many cases possess C1 point symmetry, leading to non-linear optical properties [21,22]. The tin compound $NaSn_2Cl_5$ has also been reported, which is an AB_2X_5 type compound (A= Na, K, In, Tl, NH_4; B= Sr, Sn, Pb; X= Cl, Br, I). The Sn ions are strongly distorted $SnCl_6$ trigonal prisms with three additional chlorides capping the polyhedron. Sodium is coordinated to six chlorine atoms, forming a slightly distorted octahedron, which in turn share edges with the trigonal prisms [23].

The fluoride ion conductors ($MSnF_4$) show high fluoride conductivity based on the tetragonal distortion of their cubic fluorite lattice, which arises from the presence of metal cationic species of different sizes (M= Pb, Ba, Ca) [24]. Finally, fluoride-doped tin dioxide is a transparent conductor, and is synthesized

*Corresponding author. Fax: +6077774478.
E-mail address: soliver@binghamton.edu (S.R.J. Oliver).

0022-4596/$ - see front matter © 2003 Published by Elsevier Inc.
doi:10.1016/j.jssc.2003.09.013

by sol–gel, spray pyrolysis, sputtering or chemical vapor deposition (CVD) [25]. These materials are important for their use as coatings on infrared windows.

Here, we discuss the synthesis, structure and characterization of a new sodium tin fluoride (BING-12, $NaSnF_3$) structure as well as single crystal data for a tin fluorophosphate (Compound **2**). In light of the widespread previous studies on condensed tin fluorides, it is surprising that our new compound, with such a simple chemical formula, has not been previously reported.

2. Experimental

2.1. Synthetic procedure

BING-12 ($NaSnF_3$) was synthesized solvothermally in a reaction mixture composed of the following: (i) pyridine solvent (Acros, 99%); (ii) distilled water; (iii) hydrofluoric acid (49% aqueous, Aldrich); (iv) sodium tetrafluoroborate (Gelest); (v) tin (II) oxalate (Gelest). The molar ratio was 20:4:1:1:1, respectively (Table 1). The chemicals were thoroughly stirred in a Nalgene beaker, then transferred into a 23 mL capacity Teflon-lined Parr autoclave and heated at 423 K for 7 days. The colorless plate-like crystals were rinsed with acetone under vacuum filtration and dried in air.

Compound **2** ($Sn_3F_3PO_4$) can be synthesized in distilled water, pyridine or a combination of the two, keeping the total volume constant (Table 1). The following were then added sequentially to the solvent:hydrofluoric acid (49% aqueous, Aldrich), tin (II) fluoride (Gelest) and boric acid (H_3BO_3, Aldrich). Finally, either hexafluorophosphoric acid (HPF_6, 60% aqueous, Acros) or tetra-*n*-butylammonium hexafluorophosphate [$(C_4H_9)_4NPF_6$, 98%, Acros] was added. The molar ratio and experimental conditions are listed in Table 1 (Expts. 7–11). The mixture was allowed to react in a 16 mL capacity Teflon-lined autoclave (constructed in-house). The needle-like crystals were rinsed with water under vacuum filtration and dried in air.

2.2. Characterization methods

A small amount of sample was ground in a mortar and pestle and mounted on a powder X-ray diffraction (PXRD) sample holder. The PXRD pattern was collected from 2° to 45° (2θ), step size 0.02° and scan rate 4.0°/min, on a Scintag XDS 2000 diffractometer with Cu$K\alpha$ radiation ($\lambda = 1.5418$ Å) and solid-state detector.

A suitable colorless crystal (BING-12: plate-like, $0.48 \times 0.12 \times 0.01\,mm^3$; Compound **2**: needle, $0.32 \times 0.08 \times 0.06\,mm^3$) was mechanically selected for single crystal structure determination. SC-XRD data was collected on a Bruker AXS single-crystal diffractometer with Smart Apex detector, Mo$K\alpha$ graphite monochromated radiation ($\lambda = 0.71073$ Å) and a scan width of 0.3° in ω.

A total of 2472 frames were collected for BING-12 with an exposure time of 10 s/frame using SMART [26a]. The frames were integrated with SAINT software package using a narrow-frame integration algorithm. The integration of the data using a monoclinic unit cell yielded a total of 8760 reflections to a maximum θ angle of 30.53°, of which 2041 were independent based upon the refinement of the *XYZ*-centroids of 6164 reflections with $4.8° < \theta < 61.0°$ using SAINT. Analysis of the data showed negligible decay during data collection. The crystal structure was solved by direct methods using SHELXS90 [26b] and refined to $R_1 = 0.023$ for 1763 observed reflections.

For Compound **2**, a total of 1868 frames were collected with an exposure time of 4 s/frame using SMART [26a]. The frames were integrated with the SAINT software package using a narrow-frame integration algorithm. The integration of the data using a rhombohedral unit cell yielded a total of 2233 reflections to a maximum θ angle of 30.50°, of which 754 were independent based upon the refinement of the *XYZ*-centroids of 2110 reflections with $6.9° < \theta < 62.9°$ using SAINT. The crystal structure was solved by direct methods using SHELXS90 [26b] and refined to $R_1 =$

Table 1
Summary of synthesis conditions

No.	Molar ratios (Py = pyridine, C_5H_5N)	Synthesis time (days)	Synthesis temp. (°C)	Major phase(s) observed in PXRD
1	20 Py:4 H_2O:1 HF:1 $NaBF_4$:1 Sn(C_2O_4)	7	150	BING-12
2	20 Py:4 H_2O:1 HF:1 $NaBF_4$:1 Sn(C_2O_4)	5	150	BING-1 [6]
3	80 H_2O:1 HF:1 $NaBF_4$:1 Sn(C_2O_4)	7	150	Unknown phase
4	20 Py:20 H_2O:1HF:1 $NaBF_4$:1 Sn(C_2O_4)	7	150	Unknown phase
5	20 Py:4 H_2O:1 $NaBF_4$:1 Sn(C_2O_4)	7	150	Unknown phase
6	20 Py:4 H_2O:1 HF:1 $NaBF_4$:1 Sn(C_2O_4)	7	175	Unknown phase
7	20 Py:10 H_2O:2 HF:0.25 $(C_4H_9)_4NPF_6$:1 SnF_2	5	150	Compound **2**
8	20 Py:10 H_2O:2 HF:0.25 $(C_4H_9)_4NPF_6$:1 SnF_2	5	175	Unknown phase
9	20 Py:2 HF:0.25 $(C_4H_9)_4NPF_6$:1 SnF_2	5	150	Compound **2**
10	80 H_2O:1 HF:5 H_3BO_3:0.5 HPF_6:1 SnF_2	5	150	Compound **2**
11	80 H_2O:1 HF:5 H_3BO_3:0.5 HPF_6:1 SnF_2	5	175	Unknown phase

0.021 for 738 observed reflections. All data were corrected for absorption effects with the semi-empirical from equivalents method using SADABS [26c].

In situ VT-PXRD was collected on a Phillips PW3040-MPD powder X-ray diffractometer using Cu$K\alpha$ radiation ($\lambda = 1.5418$ Å) and fitted with an Anton Parr heating stage (model HTK-10, calibrated to the melting point of Pb). The samples were ground in a ceramic mortar and a thin layer of the resultant powder was mounted on aluminum shim stock (0.0153″ thickness, ca. 1″ length and 0.5″ width) and placed on the heating stage. Typical 2θ scans were taken from 2° to 45° at a scan rate of 4.0°/min. Scans were taken at regular temperature intervals, followed by a final scan after the sample had cooled to room temperature.

Thermogravimetric analysis (TGA) was performed on a TA Instruments 2950, with a 10°C/min scan rate and oxygen purge, mounting the as-synthesized sample on the platinum sample holder. Scanning electron microscopy (SEM) data was collected on an ETEC Autoscan SEM. All specimens were first coated with a Pd–Au alloy (1:1 ratio) using a Denton Vacuum Desk 1 sputter coater. SEM operating conditions were 10 kV and 23 mm working distance.

3. Results and discussion

3.1. BING-12

Pyridine is required for the formation of this product, as more aqueous or entirely aqueous solvents resulted in unknown products (Expts. 3 and 4, Table 1). Organic solvents have been known to provide an ideal environment for synthesis of new inorganic compounds, due to properties such as viscosity, chelation and the absence of water [27]. Poeppelmeier and co-workers have shown a higher degree of protonation of pyridine in the absence of water, producing pyridinium cations needed to bring about crystallization [27a,27b,28]. The protonation may legate the metal source thereby directing the structure. Addition of more water leads to less protonation of the pyridine, resulting in a mix of unreacted materials. Pyridine has also been known to slow down reaction of metal sources, which accounts for the structural diversity with this solvent system [4–9].

Hydrofluoric acid was added as a mineralizer, along with BF_4^- as a potential anionic template (Expt. 1, Table 1).[1] Experiments carried out in the absence of HF gave no BING-12 and instead an unknown phase (Expt. 5, Table 1). Increasing the temperature also led to the formation of an unknown phase (Expt. 6, Table 1).

[1] It was not determined if HF and/or BF4—was the fluoride source for BING-12. The necessity of HF, however, implies it has a dual role in the reaction mixture, as mineralizer and structure-director.

Crystallographic parameters for BING-12 and Compound 2 are listed in Table 2. BING-12 is a layered structure (Fig. 1), with two crystallographically unique Sn centers. Each Sn is pyramidal three-coordinate, bonding to three fluoride ions [Sn–F distances range from 2.033(2) Å to 2.081(2) Å]. The fluorides in turn double or triply bridge to Na centers [Na–F bond lengths range from 2.250(2) to 2.495(2) Å]. The latter are six- and seven-coordinate and reside at the center of the layer, while the Sn centers dominate the outer edge of the layers (Fig. 1a).

The structure of the layer can be thought of as charged sodium galleries sandwiched between two tin fluoride layers to form a triple layer. The layers are separated by repulsion from lone pairs residing on the Sn centers (Fig. 1a). These outer lone pairs are commonly observed for other Sn- and Pb-based layered structures [4–9]. Selected bond angles and bond lengths are listed in Table 3. The SEM shows BING-12 has a plate-like morphology hundreds of microns across, but very thin (Fig. 2a, Table 2).

The anisotropy of the lone pairs may also give rise to interesting magnetic behavior. BING-12 may be useful as an alkali metal conductor based on its structural similarity with a tetragonal $Na_2CoP_2O_7$ reported by Sanz et al. [29]. The spaces inbetween the CoP_2O_7 layers are filled with sodium ions, the material has an ionic conductivity of 2×10^{-5} Scm^{-1} at 300°C.

Table 2
Summary of crystal data, details of intensity collection, and refinement

	BING-12	Compound **2**
Empirical formula	$NaSnF_3$	$Sn_3F_3PO_4$
Formula weight	198.68	470.04
Crystal size (mm)^3	$0.48 \times 0.12 \times 0.01$	$0.32 \times 0.08 \times 0.06$
Crystal system	Monoclinic	Rhombohedral
Space group	$C2/c$	$R3$
Color of crystal	Colorless	Colorless
a (Å)	11.7429(12)	11.8647(11)
b (Å)	17.0104(18)	11.8647(11)
c (Å)	6.8528(7)	4.6291(6)
α (deg)	87.982(2)	90.00
β (deg)	87.916(2)	90.00
γ (deg)	85.650(2)	120.00
V (Å^3)	1345.1(2)	564.34(10)
Z	16	3
T (K)	293(2)	293(2)
D_C (g cm^{-3})	3.924	4.149
Absorption coefficient, μ (mm^{-1})	7.5900	10.059
No. of observed data $[I > 2\sigma(I)]$	1763	754
$R_1[I > 2\sigma(I)]$	0.0227	0.0211
wR_2 (all data)	0.0531	0.0463
Goodness of fit on F^2	0.972	1.033
R_{int}	0.0371	0.0380
R_{Sig}	0.0292	0.0402

$R1 = \sum||F_o| - |F_c||/\sum|F_o|$, $wR2 = [\sum w(F_o^2 - F_c^2)^2/\sum w(F_o^2)^2]^{1/2}$.

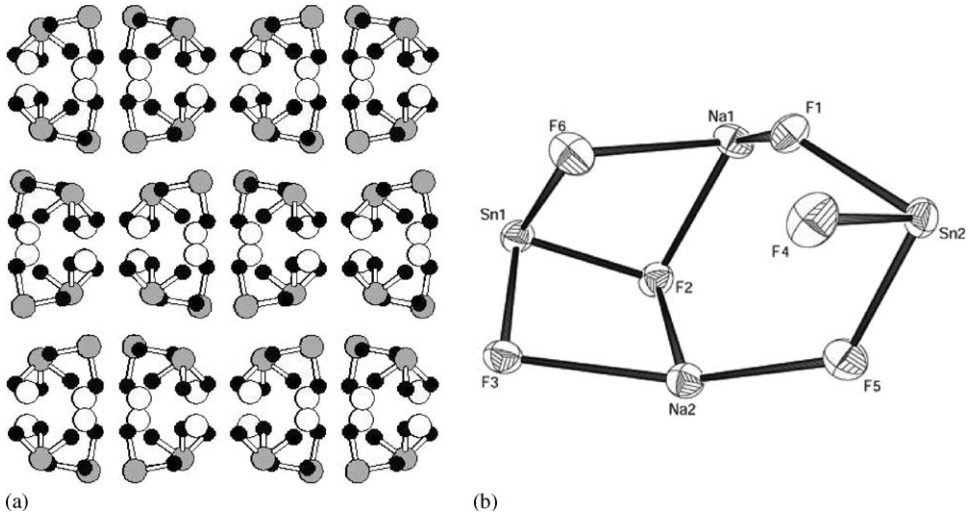

Fig. 1. The crystal structure of BING-12 ($NaSnF_3$): (a) the *c*-projection of several layers shows the outer pyramidal SnF_3 centers that cap the layers and the central charged galleries filled with Na^+ counter ions (Sn–large gray circles; Na–open circles; F–small black circles); and (b) thermal ellipsoids and atom labeling scheme, shown at 50% probability levels.

Table 3
Selected bond lengths (Å) and bond angles (deg) for each structure

BING-12		Compound **2**	
Sn(1)–F(6)	2.0333(19)	Sn(1)–F(1)	2.269(3)
Sn(1)–F(3)	2.0612(18)	F(1)–Sn(1)	2.269(3)
Sn(1)–F(2)	2.0678(19)	P(1)–O(1)	1.532(5)
Sn(2)–F(4)	2.050(2)	P(1)–O(2)	1.555(6)
Sn(2)–F(5)	2.070(2)	O(2)–P(1)	1.555(6)
Sn(2)–F(1)	2.0806(18)	Sn(1)–F(1)	2.063(3)
Sn(1)–Na(1)	3.3558(13)	Sn1–O1	2.093(4)
Sn(1)–Na(2)	3.4957(14)		
Sn(1)–Na(2)	3.7284(14)		
Sn(2)–Na(1)	3.5724(14)	O(1)–Sn(1)–F(1)	79.11(14)
Na(1)–F(1)	2.236(2)	Sn(1)–F(1)–Sn(1)	146.9(2)
Na(1)–F(2)	2.333(2)	O(1)–P(1)–O(1)	111.50(13)
Na(1)–F(6)	2.488(3)	O(1)–P(1)–O(2)	107.36(14)
Na(1)–F(4)	2.525(2)	P(1)–O(1)–Sn(1)	135.3(2)
Na(2)–F(3)	2.250(2)	F(1) Sn(1) O(1)	87.06(18)
Na(2)–F(5)	2.301(3)	F(1) Sn(1) F(1)	81.62(19)
Na(2)–F(2)	2.305(2)		
F(6)–Sn(1)–F(3)	89.27(8)		
F(6)–Sn(1)–F(2)	80.60(8)		
F(3)–Sn(1)–F(2)	82.19(7)		
F(4)–Sn(2)–F(5)	86.69(9)		
F(4)–Sn(2)–F(1)	79.84(8)		
F(5)–Sn(2)–F(1)	89.56(8)		
F(6)–Sn(1)–Na(1)	45.59(6)		
F(3)–Sn(1)–Na(1)	104.83(6)		
F(3)–Sn(1)–Na(2)	35.90(6)		
F(2)–Sn(1)–Na(2)	105.29(6)		
F(1)–Na(1)–F(1)	133.48(9)		
F(1) Na(1) F(2)	113.64(8)		

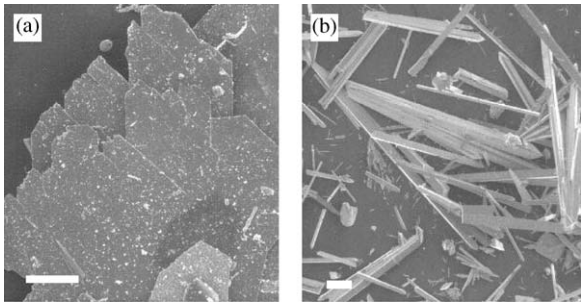

Fig. 2. SEM of the tin fluoride crystals (scale bar: 100 μm): (a) BING-12; and (b) Compound **2**.

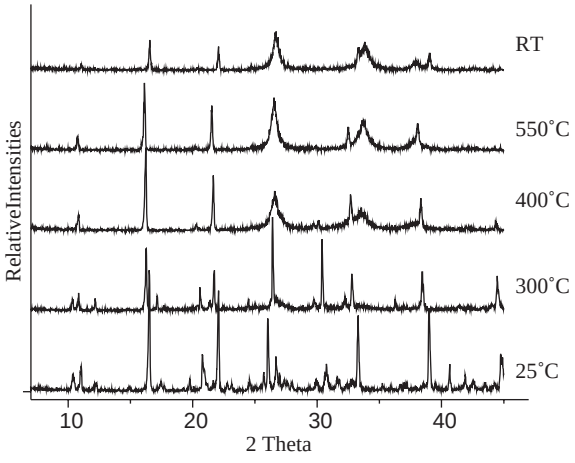

Fig. 3. In situ VT-PXRD Patterns of BING-12, indicating the phase change around 300°C.

Similarly, a sodium phosphate $Na_4Ni_5(PO_4)_2(P_2O_7)_2$, conducts Na^+ ions at 500°C, where the sodium ions reside in the tunnels defined by the NiP_2O_{22} blocks [30].

The experimental PXRD pattern of the material (Fig. 3, 25°C) matched the theoretical pattern generated from the single crystal data. The physical properties of BING-12 and Compound **2** were studied using TGA, PXRD and VT-PXRD. The TGA showed that BING-12 has little or no occluded water, as no significant weight loss was recorded at 100°C. The material

remained stable to approximately 275°C in oxygen flow. The TGA trace then showed a slight increase of 1.21 wt% around 328°C, which may be due reaction with the oxygen flow. The weight gain was followed by a sharp loss of 7.34 wt% around 500°C. The TGA trace of BING-12 shows a total loss of approximately 8.58 wt% up to 500°C. The VT-PXRD patterns in these regions where these changes occurred (328–500°C) showed no changes despite the loss and gain in weight. The broad peaks in the higher temperature patterns correspond to tin oxide (cassiterite form of SnO_2, JC-PDS ref. 02-1340) (Fig. 3).

3.2. Compound 2, Sn_3F_3PO4

Compound **2** can be synthesized with one of two different phosphate sources, HPF_6 or $(C_4H_9)_4NPF_6$.[2] The synthesis is not pyridine-specific, and can be carried our in a pyridine–water solvent mixture or only in water (Expts. 7, 9 and 10, Table 1). Boric acid is not incorporated in the crystalline product; it was used to give better quality crystals, likely through control of nucleation rate. Others have observed and proposed the same phenomenon with H_3BO_3 in the reaction medium [31]. Our crystallographic data ($R_1 = 2.16\%$, $wR_2 = 4.63\%$, Table 2) is a vast improvement over the original report for this compound ($R = 7.6\%$) [32]. Their synthesis was carried out by a precipitation technique using hydroxyapatite $[Ca_5(PO_4)_3OH]$ and tin fluoride. In addition, our product was phase pure, while their product was predominantly CaF_2, with only some $Sn_3F_3PO_4$.

The framework of Compound **2** is made up of helical –Sn–F–chains, which run along the *c*-axis in a clockwise manner (Fig. 4a). Two vertices of the three-coordinate Sn centers belong to the chain, while the third vertex is the oxygen of the phosphates, which connect the chains to define a framework (Fig. 4b). The phosphate has three of its oxygen's bridging to neighboring tin centers while the fourth is terminal and points parallel to the *c*-axis. The Sn–O [2.093(4) Å] and Sn–F [2.063(3)–2.069(3) Å] bonds are strong, and the P–O bonds [1.532(5)–1.555(6) Å] are typical for a phosphate group. Selected bond angles and bond lengths for both BING-12 and Compound **2** are listed in Table 3.

Judging from the TGA and VT-PXRD data, Compound **2** remained stable until 350°C, where a weight loss of ~1.31 wt% occurred. A gain in weight of 3.83 wt% was then recorded around 400°C, due to reaction with oxygen. The VT-PXRD pattern remained the same from 350°C to 550°C, the peaks again fitting well with the cassiterite form of SnO_2 (JC-PDS ref. 02-1340). Additional peaks that were observed likely belong to $Sn_2P_2O_7$ (JC-PDS ref. 35-0028). The SEM of Compound **2** shows a well-defined crystal habit (Fig. 2b), the needle-like morphology reflecting the chain character of the building block of the compound.

[2] We have not yet determined if phosphoric acid and HF may be used in place of hexafluorophosphate.

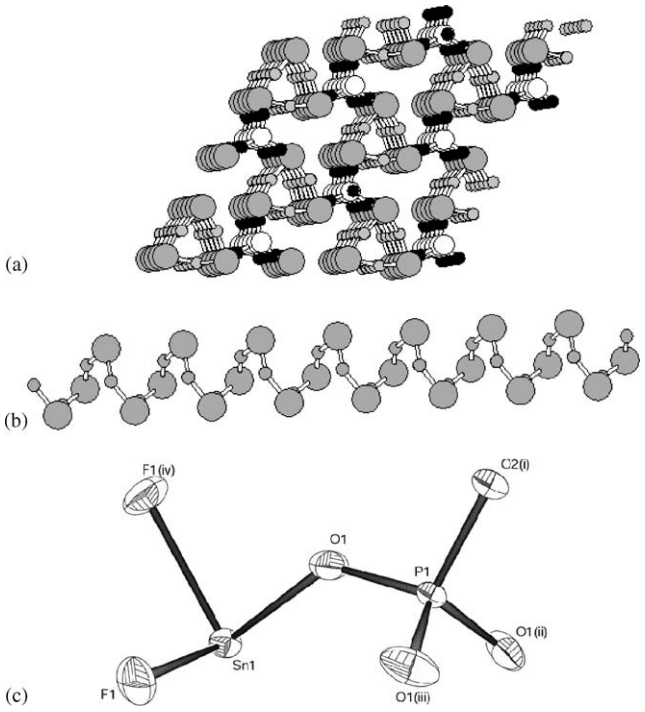

Fig. 4. The crystal structure of Compound **2**, $Sn_3F_3PO_4$: (Sn–large gray circles, P–open circles, F–small gray circles, O–black circles) (a) the *c*-projection of the –Sn–F–helical chains connected by phosphate ions; (b) *b*-projection of compound **2**, with omission of phosphate groups to emphasize the helical –Sn–F–chains; and (c) thermal ellipsoids and labeling scheme, shown at 50% probability levels, (i) $x, y, z-1$ (ii) $-y+z, x-y+1, z$ (iii) $-x+y+1, -x+z, z$ (iv) $-x+y+1/3, -x+2/3, z-1/3$.

4. Conclusions

A new type of tin fluoride (BING-12) and a previously reported tin fluorophosphate have been synthesized in a water–pyridine solvent system. Compound 2 shows drastically improved crystallographic data compared to that previously reported. These compounds add to the diverse and interesting chemistry of tin fluoride compounds. It is our hope that apart from the numerous chain and open framework compounds isolated from our system thus far, we will be able to develop a scheme to synthesize channel compounds with tunable pore size and shape for molecular sieve applications.

Acknowledgments

This work was supported by an NSF CAREER Award, 2003–2008 (DMR-0239607). We are also

grateful to Henry Eichelberger, Department of Biology, for help with SEM images, as well as Dr. Jenkins of the Department of Geology for use of the VT-XRD machine and help with data collection.

References

[1] S. Ayyappan, J.-S. Chang, N. Stock, R. Hatfield, C.N.R. Rao, A.K. Cheetham, Int. J. Inorg. Mater. 2 (1) (2000) 21–27.
[2] M.L. Elidrissi Moubtassim, J.I. Corredor, J.L. Tirado, C. Pérez Vicente, Electrochim. Acta 47 (2001) 489–493.
[3] S.M. Patel, U.V. Chudasama, P.A. Ganeshpure, J. Molecular Catal.: A Chem. 194 (1–2) (2003) 267–271.
[4] T.O. Salami, K. Marouchkin, P.Y. Zavalij, S.R.J. Oliver, Chem. Mater. 14 (2002) 4851–4857.
[5] D.T. Tran, P.Y. Zavalij, S.R.J. Oliver, J. Am. Chem. Soc. 124 (2002) 3966–3969.
[6] T.O. Salami, P.Y. Zavalij, S.R.J. Oliver, Acta Cryst. E 57 (2001) m111–m113.
[7] T.O. Salami, P.Y. Zavalij, S.R.J. Oliver, Acta Cryst. E 57 (2001) i49–i51.
[8] D.E. Lansky, P.Y. Zavalij, S.R.J. Oliver, Acta Cryst. C 57 (2001) 1051–1052.
[9] D.T. Tran, Y.-S. Kam, P.Y. Zavalij, S.R.J. Oliver, Inorg. Chem. 42 (6) (2003) 2165–2172.
[10] N. Stock, G.D. Stucky, A.K. Cheetham, Chem. Commun. (2000) 2277–2278.
[11] S. Natarajan, R. Vaidhyanathan, C.N.R. Rao, S. Ayyappan, A.K. Cheetham, Chem. Mater. 11 (1999) 1633–1639.
[12] S. Ayyappan, A.K. Cheetham, S. Natarajan, C.N.R. Rao, Chem. Mater. 10 (1998) 3746–3755.
[13] S. Ayyappan, A.K. Cheetham, S. Natarajan, C.N.R. Rao, J. Solid State Chem. 139 (1998) 207–210.
[14] S. Natarajan, A.K. Cheetham, J. Solid State Chem. 134 (1997) 207–210.
[15] B. Adair, S. Natarajan, A.K. Cheetham, J. Mater. Chem. 8 (1998) 1477–1479.
[16] S. Natarajan, M. Eswaramoorthy, S. Ayyappan, X. Bu, A.K. Cheetham, C.N.R. Rao, Chem. Mater. 10 (1998) 3308–3310.
[17] S. Ayyappan, X. Bu, A.K. Cheetham, S. Nataranjan, Chem. Commun. 20 (1998) 2181–2182.
[18] S. Ayyappan, A.K. Cheetham, C.N.R. Rao, Chem. Mater. 10 (1998) 1627–1631.
[19] S. Natarajan, A.K. Cheetham, J. Solid State Chem. 140 (1998) 435–439.
[20] S. Natarajan, M. Eswaramoorthy, A.K. Cheetham, C.N.R. Rao, Chem. Commun. 15 (1998) 1561–1562.
[21] T. Jiang, G.A. Ozin, J. Mater. Chem. 8 (5) (1998) 1099–1108.
[22] D.A. Cleary, R.D. Willett, F. Ghebremicheal, M.G. Kuzyk, Solid State Commun. 88 (1993) 39–41.
[23] Z. Zhang, H.D. Lutz, J. Solid State Chem. 115 (1) (1995) 158–164.
[24] G. Denes, Y.H. Yu, T. Tyliszczak, A.P. Hitchcock, J. Solid State Chem. 104 (1993) 239–252.
[25] D. Boegeat, B. Jousseaume, T. Toupance, G. Campet, L. Fournes, Inorg. Chem. 39 (2000) 3924–3927.
[26] (a) Bruker Smart, Saint Bruker, AXS Inc., Madison, Winconsin, USA, 1999;
(b) G.M. Sheldrick, Acta Cryst. A 46 (1990) 467–473;
(c) G.M. Sheldrick, SADABS, SHELXL97 and XPREP. University of Gottingen, 1996.
[27] (a) C. Wang, Y.D. Li, G.H. Zhang, J. Zhuang, G.Q. Shen, Inorg. Chem. 39 (2000) 4237–4239;
(b) P. Halasyamani, M.J. Willis, C.L. Stern, P.M. Lundquist, G.K. Wong, K.R. Poeppelmeier, Inorg. Chem. 35 (1996) 1367–1371;
(c) S. Oliver, A. Kuperman, G.A. Ozin, Angew. Chem. Int. Ed. Engl. 37 (1998) 46–62.
[28] P. Halasyamani, K.R. Heier, A.J. Norquist, C.L. Stern, K.L. Poeppelmeier, Inorg. Chem. 37 (1998) 369–371.
[29] F. Sanz, C. Parada, J.M. Rojo, C. Ruiz-Valero, R. Saez-Puche, J. Solid State chem. 145 (1999) 604–611.
[30] F. Sanz, C. Parada, J.M. Rojo, C. Ruiz-Valero, Chem. Mater. 11 (1999) 2673–2679.
[31] W.T.A. Harrison, M.L.F. Philips, T.M. Nenoff, E.J. Maclean, S.J. Teat, R.S. Maxwell, J. Chem. Soc. Dalton Trans. (2001) 546–549.
[32] F. Berndt, J. Dent. Res. 51 (1) (1972) 53–57.